Mathieu functions, a visual approach

J. C. Gutiérrez-Vega[a] and R. M. Rodríguez-Dagnino
Instituto Tecnológico y de Estudios Superiores de Monterrey, 64849 Monterrey NL, México

M. A. Meneses-Nava
Centro de Investigaciones en Optica, 37150 León, Guanajuato, México

S. Chávez-Cerda
Instituto Nacional de Astrofísica, Óptica y Electrónica, 72000 Puebla, México

(Received 25 June 2002; accepted 26 September 2002)

The behavior of the Mathieu functions is illustrated by using a variety of plots with representative examples taken from mechanics. We show how Mathieu functions can be applied to describe standing, traveling, and rotating waves in physical systems. Some background is provided on notation and analogies with other mathematical functions. Our goal is to increase the familiarity with Mathieu functions in the scientific and academic community using visualization. For this purpose we adopt a strategy based on visual recognition rather than only looking at equations and formulas.
[DOI: 10.1119/1.1522698]

I. INTRODUCTION

Increasing attention is being given to scientific and engineering problems that lead to differential equations of the Mathieu type.[1] Their solutions, known as Mathieu functions, were first discussed by Mathieu in 1868 in the context of the free oscillations of an elliptic membrane.[2] These functions were further investigated by a number of researchers who found a considerable amount of mathematical results that were collected more than 60 years ago by McLachlan.[3] During the last decade there have been several articles devoted to new analytical results, numerical techniques, and applications.[4–9]

Mathieu equations occur in two main categories of physical problems. First, in applications involving elliptic geometries, for example in the analysis of the vibrating modes in elliptic membranes, the propagating modes in elliptic pipes, and the oscillations of water in a lake of elliptic shape. Mathieu equations arise after separating the wave equation using elliptic coordinates.[10,11] Second, Mathieu equations arise in problems involving periodic motion, such as the trajectory of an electron in a periodic array of atoms, the mechanics of the quantum pendulum, and the oscillations of floating vessels.[12–17]

Despite the existence of many applications, what attracts our attention is that Mathieu functions are barely mentioned in modern textbooks of mathematics for physics and engineering,[18] others just present a limited discussion,[19–23] and older texts that gave some account of Mathieu functions are now out of print.[3,24–26] Nevertheless, when facing a problem that leads to the Mathieu differential equations, we can always consult the invaluable handbooks by Abramowitz and Stegun[27] and by Gradshteyn and Ryzhik.[28] However, this experience can be rather painful if one is trying to learn about Mathieu functions for the first time. In most books we find a high density of equations which, from a didactic point of view, can be scary for the unfamiliar reader.

We believe that this lack of literature compared to that for other special functions is because the behavior of Mathieu functions is relatively rich and consequently more difficult to understand. Moreover at least five different nomenclatures are in use (see Appendix A), and the computation of the Mathieu functions and their eigenvalues still presents some numerical difficulties.[8,9]

The purpose of this article is to facilitate the understanding of some of the qualitative features of Mathieu functions and their applications. We believe that the visualization of Mathieu functions will be helpful in achieving a better comprehension of their basic characteristics. This work is intended for students, teachers, and researchers who are unfamiliar with Mathieu functions, and who are interested in gaining visual insight. We shall restrict ourselves to including the minimum formulas needed to explain the basic characteristics, the different notation, and the classification of these functions. The behavior of the Mathieu functions is illustrated by using a variety of plot types with representative examples taken from mechanics. We show how Mathieu functions can be applied to describe standing, traveling, and rotating waves in physical systems.

II. VISUALIZING MATHIEU FUNCTIONS

Over the years the visualization of Mathieu functions has been limited to simple curves for a few values of their parameters. Jahnke and Emde[29] were perhaps the first authors to include three-dimensional surface representations of the Mathieu functions, whereas Abramowitz and Stegun[27] provide many useful two-dimensional plots. At present, more sophisticated computational tools are available, and hence far more complicated behavior of Mathieu functions can be explored in a variety of two- and three-dimensional plots.

If the two-dimensional Helmholtz equation

$$\frac{\partial^2 U}{\partial x^2}+\frac{\partial^2 U}{\partial y^2}+k^2U=0, \tag{1}$$

is transformed from rectangular coordinates (x,y) to elliptic coordinates (ξ,η) by the formulas

$$x=f\cosh\xi\cos\eta, \quad y=f\sinh\xi\sin\eta, \tag{2}$$

and a solution of the form $U=R(\xi)\Phi(\eta)$ is sought, it is found that $R(\xi)$ and $\Phi(\eta)$ must satisfy the equations

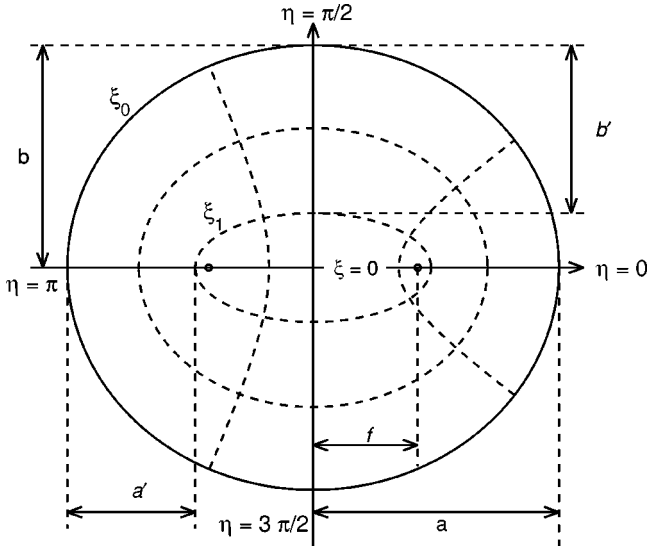

Fig. 1. Elliptic cylindrical coordinate system. The curves $\xi=$ constant are confocal ellipses and the curves $\eta=$ constant are orthogonal hyperbolas.

$$\frac{d^2\Phi}{d\eta^2}+(a-2q\cos 2\eta)\Phi=0, \tag{3}$$

$$\frac{d^2R}{d\xi^2}-(a-2q\cosh 2\xi)R=0, \tag{4}$$

where $q=f^2k^2/4$ and a is the separation constant arising from the eparation of variables method. In the literature, Eqs. (3) and (4) are known as the ordinary and the modified Mathieu equations, respectively.[27] However, in applications involving the Helmholtz equation in elliptic coordinates, Eqs. (3) and (4) are better identified as the angular and the radial Mathieu equations.[24] Their solutions are the angular Mathieu functions (AMF) and the radial Mathieu functions (RMF), respectively. This nomenclature becomes obvious when we observe in Fig. 1 the similarity between the elliptic coordinates (ξ,η) and the polar coordinates. The elliptic variable η has a domain $0\leqslant\eta<2\pi$ and plays a similar role to a polar angle, whereas the variable ξ, with domain $0\leqslant\xi<\infty$ behaves as a radial variable. The line joining the foci $(\pm f,0)$ corresponds to $\xi=0$. Notice that the polar coordinates could be considered to be a special case of the elliptic coordinates in the limit $f\to 0$ when the foci of the elliptic coordinates collapse to a point at the origin. In this limit, the angular and the radial Mathieu equations become the well-known harmonic equation and the Bessel equation, respectively.[3,27] As a consequence, the angular Mathieu functions transform into the trigonometric functions $\cos\eta$ and $\sin\eta$ and the radial Mathieu functions become the Bessel functions.

A. Angular Mathieu functions

The angular Mathieu equation (3) is a linear second-order differential equation that has two families of independent solutions, namely the even and the odd angular Mathieu functions,

$$\Phi_m=\begin{cases}\mathrm{ce}_m(\eta;q), & m=0,1,2,\ldots,\\ \mathrm{se}_m(\eta;q), & m=1,2,3,\ldots,\end{cases} \tag{5}$$

where m is the order. The notation ce and se comes from cosine-elliptic and sine-elliptic, and was first suggested by Whittaker.[22] Nowadays, it is a widely accepted notation for the AMF (see Appendix A).

The behavior of Mathieu functions is fairly complicated, particularly because we need to understand both the variable η and the parameter q dependence of the functions. Physical considerations are usually such that AMF are periodic[30] with period π or 2π. The values of a in Eq. (3) that satisfy this condition are the eigenvalues of the equation; for ce_m the eigenvalues are usually denoted as $a_m(q)$, whereas for se_m they are represented as $b_m(q)$. According to the Sturm–Liouville theory,[18] the eigenvalues form an infinite set of countable real values that have the property $a_0<b_1<a_1<b_2\cdots$. Each function ce_m and se_m is associated with an eigenvalue a_m or b_m which in turn depends on q.

In Fig. 2 we plot the functions $\mathrm{ce}_m(\eta;q)$ and $\mathrm{se}_m(\eta;q)$ for several values of m over the plane (η,q).[31] Note that Eq. (3) becomes the harmonic equation when $q\to 0$, when it is evident that ce_m and se_m become equal to the trigonometric functions $\cos m\eta$ and $\sin m\eta$ as q vanishes. The range of the plots has been limited to $[0,\pi]$, because their entire behavior can be deduced from the parity and symmetry relations provided in Table I.

The parity, periodicity, and normalization of the AMF are exactly the same as their trigonometric counterparts. This is, ce_m is even and se_m is odd, and they have period π when m is even or period 2π when m is odd. The AMF have m real zeros in the open interval $\eta\in(0,\pi)$, but they cluster around $\pi/2$ as q increases. The normalization for the AMF is

$$\int_0^{2\pi}\mathrm{ce}_p\mathrm{ce}_q\,d\eta=\int_0^{2\pi}\mathrm{se}_p\mathrm{se}_q\,d\eta=\begin{cases}\pi & \text{if } p=q,\\ 0 & \text{if } p\neq q.\end{cases} \tag{6}$$

The physical meaning of the parameter q depends on each application. For instance, the classical problems of the vibrating modes in an elliptic membrane[10] and the probability distributions in an elliptic quantum billiard[32] are mathematically equivalent, that is, in both cases Mathieu equations arise after separating the wave equation or Schrödinger equation in elliptic coordinates. However, as we will discuss below, in the first case q is related to the eigenfrequencies of the vibrating modes, whereas in the second case q is associated with the characteristic energies of the eigenstates in the billiard.

An interesting one-dimensional example where the AMF occur is the quantum pendulum.[14–16] Consider a plane pendulum of length L and mass M oscillating under the action of gravity. The time-independent Schrödinger equation corresponding to this problem is

$$-\frac{\hbar^2}{2ML^2}\frac{d^2\Psi}{d\theta^2}+[V(\theta)-E]\Psi=0, \tag{7}$$

where θ is the angular displacement from the vertical, $V(\theta)=-MgL\cos\theta$ is the potential energy, and $\Psi(\theta)$ is the wave function associated with the energy E. The boundary condition to be imposed on Ψ is that it be single valued in θ, that is, $\Psi(\theta)$ has period 2π: $\Psi(\theta+2\pi)=\Psi(\theta)$. Equation (7) can be rewritten in the form of an angular Mathieu equation (3), by defining

$$\theta=2\eta, \tag{8a}$$

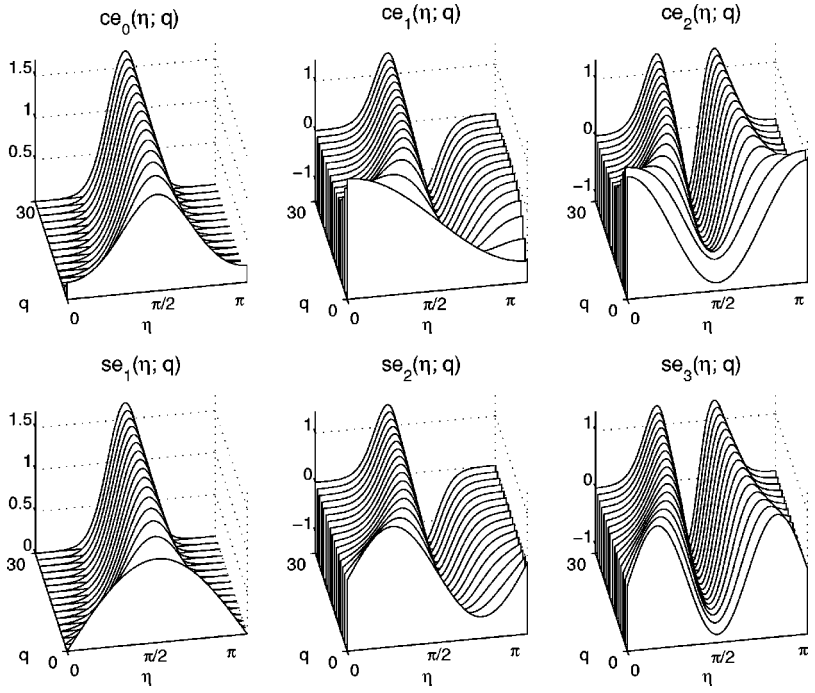

Fig. 2. Graphical visualization of angular Mathieu functions $\mathrm{ce}_m(\eta;q)$ and $\mathrm{se}_{m+1}(\eta;q)$ over the (η,q) plane. The function $\mathrm{ce}_0(\eta;q)$ is never negative, although oscillatory.

$$a=\frac{4E}{(\hbar^2/2ML^2)}, \tag{8b}$$

$$q=-\frac{2MgL}{(\hbar^2/2ML^2)}. \tag{8c}$$

In view of Eq. (8a), the boundary condition is $\Psi[2(\eta+\pi)]=\Psi[2\eta]$, that is, as a function of η, the wave function has to be periodic with period π. From Table I, such solutions are AMF of even order: $\mathrm{ce}_{2r}(\eta;q)$ and $\mathrm{se}_{2r+2}(\eta;q)$ for $r=0,1,2,\ldots$. All other AMF are excluded by the periodicity condition. We note further that characteristic values of the energy E_m are defined by the eigenvalues a_m of the Mathieu equation; from Eq. (8b) we find $E_m(\hbar^2/8ML^2)a_m$.

Also, we can see from Eq. (8c) that, for the quantum pendulum, the parameter q depends only on the given physical constants of the problem, and that Eq. (7) really corresponds to a Mathieu equation with negative q. To satisfy the usual definition of the Mathieu functions, we must perform the change of variable $\eta\rightarrow(\pi/2-\eta)$ according to Table I.

When visualizing mathematical functions, a suitable plot depends on the purpose. For example, the surfaces shown in Fig. 2 were done following a mathematical point of view. These diagrams allow us to appreciate at a glance the evolution of ce and se as functions of η or q. In Fig. 3 we adopt a physical point of view to show the probability distributions Ψ^2 of the quantum pendulum. As stated, the wave functions are written in terms of AMF of even order, $\mathrm{ce}_{2r}(\eta;q)$ and $\mathrm{se}_{2r+2}(\eta;q)$. We might plot these solutions against the polar coordinate θ in a rectangular system (θ,Ψ^2), but a more meaningful picture is usually a polar diagram. In Fig. 3, we can visualize how the probability distributions of a quantum pendulum vary with θ.

B. Radial Mathieu functions

The solutions of Eq. (4) when q is positive are the even (e) and odd (o) oscillatory radial Mathieu functions of the first and second kind,

$$R=\begin{cases}\mathrm{Je}_m(\xi;q), \quad \mathrm{Jo}_m(\xi;q), & \textit{first} \text{ kind},\\ \mathrm{Ne}_m(\xi;q), \quad \mathrm{No}_m(\xi;q), & \textit{second} \text{ kind}.\end{cases} \tag{9}$$

For $q<0$ the solutions are known as the evanescent radial Mathieu functions

$$R=\begin{cases}\mathrm{Ie}_m(\xi;q), \quad \mathrm{Io}_m(\xi;q), & \textit{first} \text{ kind},\\ \mathrm{Ke}_m(\xi;q), \quad \mathrm{Ko}_m(\xi;q), & \textit{second} \text{ kind}.\end{cases} \tag{10}$$

In elliptic coordinates the radial Mathieu equation (4) plays a similar role as the Bessel equation in circular cylindrical coordinates. Because Bessel functions are better known than Mathieu functions, visualizing their analogies is a practical way to gain an insight into the qualitative behav-

Table I. Symmetry relations for AMF.

Function $r=0,1,\ldots$	Period	Parity about $\eta=0$	Parity about $\eta=\pi/2$	AMF with $q<0$
$\mathrm{ce}_{2r}(\eta;q)$	π	Even	Even	$\mathrm{ce}_{2r}(\eta;-q)=(-1)^r\mathrm{ce}_{2r}(\pi/2-\eta;q)$
$\mathrm{ce}_{2r+1}(\eta;q)$	2π	Even	Odd	$\mathrm{ce}_{2r+1}(\eta;-q)=(-1)^r\mathrm{se}_{2r+1}(\pi/2-\eta;q)$
$\mathrm{se}_{2r+2}(\eta;q)$	π	Odd	Even	$\mathrm{se}_{2r+2}(\eta;-q)=(-1)^r\mathrm{se}_{2r+2}(\pi/2-\eta;q)$
$\mathrm{se}_{2r+1}(\eta;q)$	2π	Odd	Odd	$\mathrm{se}_{2r+1}(\eta;-q)=(-1)^r\mathrm{ce}_{2r+1}(\pi/2-\eta;q)$

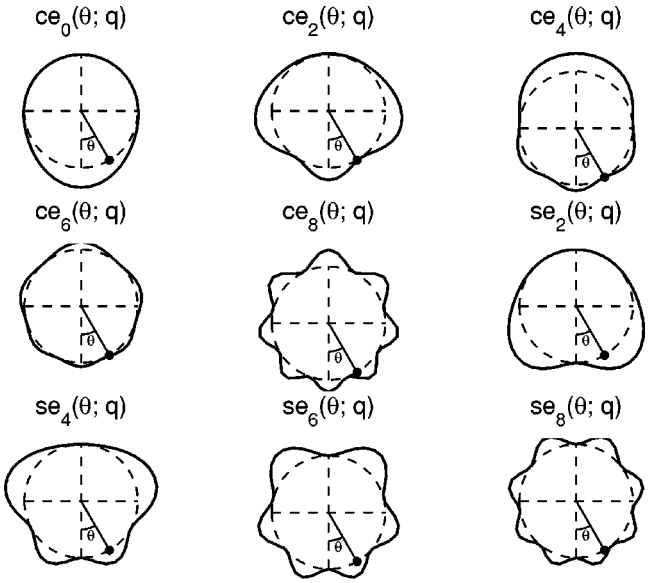

Fig. 3. Polar diagrams of the probability distributions of a quantum pendulum as a function of θ.

ior of the RMF. It is known that Bessel equations have four families of independent solutions,[18] namely the ordinary Bessel functions J_m and N_m, and the modified Bessel functions I_m and K_m. Each Bessel family splits into two Mathieu families, for example, the Bessel function J_m splits into the even Je_m and the odd Jo_m Mathieu functions. Thus there are eight independent families of RMF. This abundance of elliptic solutions has provoked confused notations in the literature which often complicates the recognition of the RMF and their relations. We refer the interested reader to Appendix A, where a comparative table of notation for the Mathieu functions is provided.

In Fig. 4 we show the first-order RMF for different values of q. Similar to the Bessel functions, the RMF have a decreasing, oscillatory non-periodic behavior. Conversely to the AMF, the radial solutions oscillate faster as q increases. In Fig. 5 we plot the RMF Je_0 for $q=5$ in two different views. Adopting a mathematical point of view, we show in Fig. 5(a) Je_0 as a function of the argument ξ. The Bessel analogy of Je_0 is indeed the lowest-order Bessel function J_0. Like J_0, the function Je_0 is oscillatory, decreasing, and non-periodic. By comparing Je_0 with respect to J_0, we can observe that the maximum at the origin of Je_0 is not as dominant as in the case of J_0, and that Je_0 oscillates faster as ξ increases.

Figure 5(b) shows again Je_0, but now physical insight is gained by plotting it as a function of $\sinh(\xi)$ instead of ξ. For instance, as we will see below, Je_0 could represent the radial dependence of a vibrating mode in an elliptic membrane.[10] In this case the argument ξ is associated with the radial elliptic coordinate (which is dimensionless). However, to visualize the spatial behavior of the mode, it is required to plot it against a coordinate with a length dimension such as x or y. Let us consider the y axis. By setting $\eta=\pi/2$ in Eq. (2), it is clear that the y axis is written as $y=f\sinh\xi$. In this manner, the plot in Fig. 5(b) could show the behavior of the vibrating mode as a function of the normalized coordinate y/f.

The plot in Fig. 5(b) reveals an important property of the radial Mathieu functions: they tend to be damped periodic functions when they are plotted against a spatial coordinate like $x\sim\cosh\xi$ or $y\sim\sinh\xi$. This characteristic is interesting because often the physical patterns are associated with the asymptotic behavior of the mathematical functions.

III. VISUALIZING STANDING WAVES IN AN ELLIPTIC MEMBRANE

As stated, the angular and the radial Mathieu equations can be expected to appear in any problem involving the Helmholtz equation expressed in elliptic coordinates.[10,32] Consider the free oscillations of an elliptic membrane with

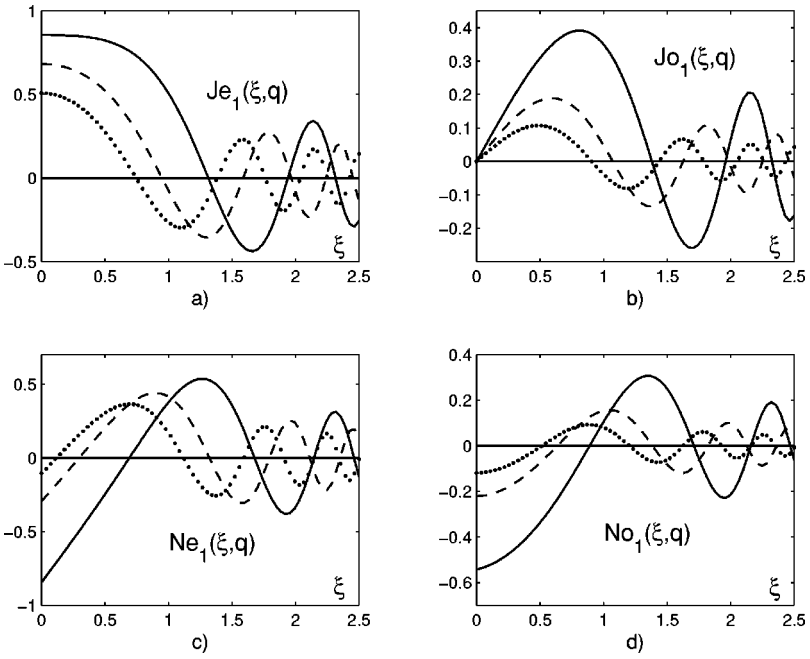

Fig. 4. Plots of radial Mathieu functions with $q=1$ (solid line), $q=2$ (dashed line), and $q=3$ (dotted line).

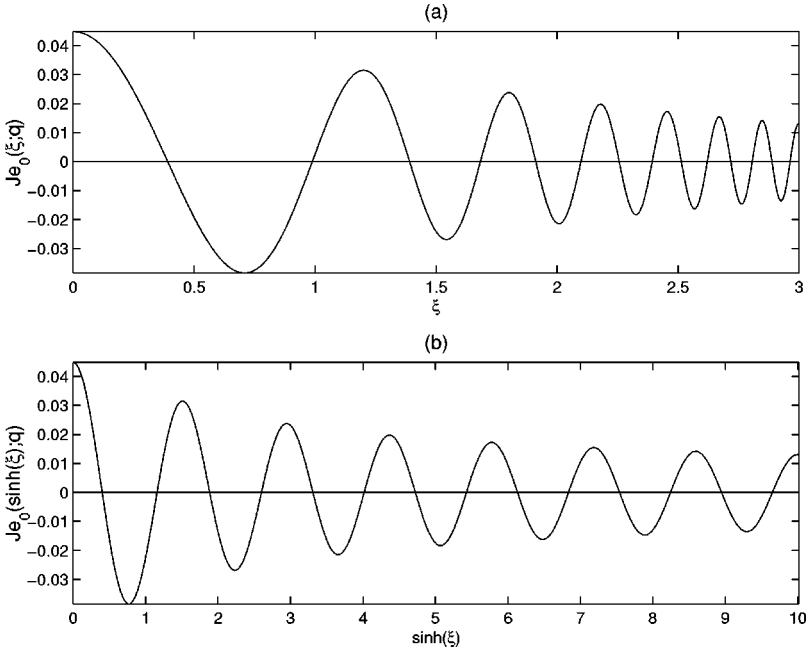

Fig. 5. Two views of the Je_0 radial Mathieu function: (a) plotted against ξ (mathematical view), and (b) plotted against $\sinh \xi$ (physical view).

semiaxes a and b, and focal distance f (see Fig. 1). The boundary of the membrane is expressed in elliptic coordinates as $\xi=\xi_0=\arctan h(b/a)=$constant.

If $Z(x,y,t)$ is the vertical displacement as a function of time of a point located at $(x.y)$, then Z satisfies the two-dimensional wave equation

$$\frac{\partial^2 Z}{\partial x^2}+\frac{\partial^2 Z}{\partial y^2}=\frac{1}{v^2}\frac{\partial^2 Z}{\partial t^2}, \tag{11}$$

where $v^2=F/\sigma$, with σ the surface mass density and F the uniform tension per unit length in each point of the membrane. By assuming a harmonic time dependence $Z(x,y,t)=U(x,y)\cos(\omega t)$, the wave equation becomes the Helmholtz equation (1), where $k=\omega/v$. After applying Eq. (2) to transform the Helmholtz equation into elliptic coordinates, and taking the separable solution $U(\xi,\eta)=R(\xi)\Phi(\eta)$, we obtain the angular and the radial Mathieu equations (3) and (4). In this case, the parameter q is given by

$$q=\frac{f^2}{4}k^2=\frac{f^2}{4}\frac{\omega^2}{v^2}=\frac{f^2\omega^2\sigma}{4F}. \tag{12}$$

A vibrating mode can be considered as a standing wave, that is, each point on the surface vibrates harmonically with an amplitude $U(x,y)$, but all points have the same frequency. The modes are given by appropriate products of radial and angular Mathieu functions, namely, the even Ze_m and odd Zo_m solutions:[33]

$$\mathrm{Ze}_m=\mathrm{Je}_m(\xi;q)\,\mathrm{ce}_m(\eta;q)\cos(\omega_m t), \tag{13}$$

$$\mathrm{Zo}_m=\mathrm{Jo}_m(\xi;q)\,\mathrm{se}_m(\eta;q)\cos(\omega_m t), \tag{14}$$

where $m\geqslant 0$ for even modes, and $m\geqslant 1$ for the odd ones. These wave solutions must satisfy the Dirichlet condition at the elliptic boundary, that is, $Z(\xi_0,\eta,t)=0$. This occurs only if the radial functions vanish at the boundary, namely,

$$\mathrm{Je}_m(\xi_0,q)=\mathrm{Jo}_m(\xi_0,q)=0. \tag{15}$$

As seen in Figs. 4 and 5, the RMF are decreasing-oscillatory nonperiodic functions. As a consequence, for a given order m, there are an infinite set of possible values of q that satisfy Eq. (15). Let $q_{m,n}$ be the nth zero ($n=1,2,\ldots$) of the radial functions Je_m or Jo_m. According to Eq. (12) for each $q_{m,n}$, there exists a corresponding eigenfrequency given by $\omega_{m,n}=(4Fq_{m,n}/\sigma f^2)^{1/2}$.

In Fig. 6 we show the first even and odd vibrating modes in the elliptic membrane. Notice the symmetry and the antisymmetry with respect to the x axis of the even and odd modes, respectively. The radial nodal lines (elliptic lines) are defined by the zeros of the radial functions e_m and Jo_m, whereas the zeros of the angular functions ce_m and se_m define the angular nodal lines (straight or hyperbolic lines). We can see that $U_{m,n}$ has m angular nodal lines and n radial

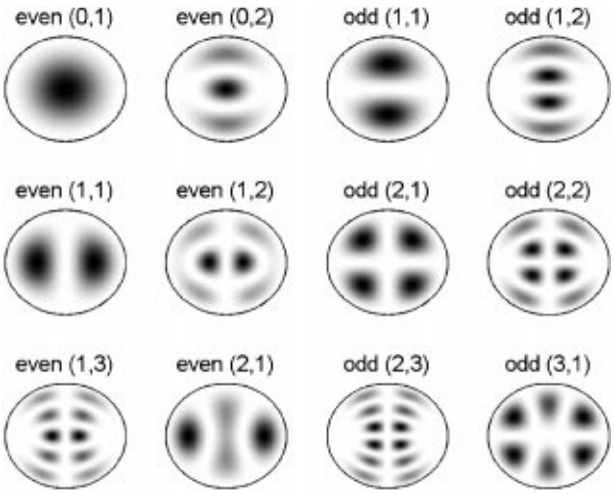

Fig. 6. Plots of the first even and odd standing modes in an elliptic membrane. The shaded regions represent crests (maxima) or valleys (minima) on the membrane surface. For instance, the even mode Ze_{11} presents one crest and one valley.

Table II. Eigenfrequencies $\omega_{m,n}$ in rad/s for the circular and the elliptic membranes; $a=5$ cm, $b=3$ cm.

Order	Circular		Even elliptic		Odd elliptic	
m	$n=1$	$n=2$	$n=1$	$n=2$	$n=1$	$n=2$
0	48.1	110.4	65.9	168.5		
1	76.6	140.3	91.5	191.2	116.5	220.7
2	102.7	168.3	118.9	215.0	139.8	243.0

Table III. Eigenfrequencies in $\sqrt{4gd/f^2}$ units.

	${}_e\omega_{m,n}$			${}_o\omega_{m,n}$		
m	$n=1$	$n=2$	$n=3$	$n=1$	$n=2$	$n=3$
0	0	1.0849	2.0583			
1	0.3508	1.2748	2.2629	0.3151	1.1017	2.0588
2	0.6458	1.4586	2.4499	0.6396	1.3667	2.2693
3	0.9222	1.6973	2.6099	0.9213	1.6665	2.4875

nodal lines including the boundary as a nodal line. The cross points between radial and angular nodal lines correspond to nodal points of the membrane. In particular, the mode $U_{m,n}$ has $m+4m(n-1)$ nodal points. The origin is a nodal point of $U_{m,n}$ only if m is odd.

To gain some intuition about the numerical values involved, we show in Table II the first natural frequencies for an elliptic membrane with $a=5$ cm, and $b=3$ cm. To make appropriate comparisons, the corresponding eigenfrequencies for a circular membrane with radius $a=5$ cm are included as well.[34] For numerical purposes, without loss of generality, we have choose the tension and density of the membrane such that $\sqrt{F/\sigma}=1$. Note that for each circular mode, there are two corresponding elliptic modes, the even one and the odd one. From Table II we can see that, for a given $U_{m,n}$, the even and odd modes vibrate with different frequencies, in fact, the even modes have lower frequencies than the odd modes. The reason is that the even modes vibrate along the largest axis of the ellipse, whereas odd modes vibrate along the shortest axis.

IV. VISUALIZING TRAVELING AND ROTATING WAVES IN AN ELLIPTIC LAKE

Finding the oscillations of water in an elliptic lake is a classic problem. The oldest references to this problem may date back to 1924 and 1927 by Jeffreys[35] and Goldstein,[36] respectively. To show the interesting phenomenon of rotating waves inside the lake, we extend their analysis by including a confocal elliptical wall inside the lake.

The geometry of the confocal annular elliptic lake is shown in Fig. 1. In terms of elliptic coordinates, the inner and outer walls correspond to curves $\xi=\xi_1=$constant and $\xi=\xi_0=$constant, respectively. If $Z(\xi,\eta,t)$ is the vertical displacement of the water surface from its equilibrium position, then Z satisfies the wave equation (11), but now $v^2=gd$, where g is the acceleration due to gravity and d is the undisturbed depth. By following the same procedure described above for the membrane, the oscillating modes in the lake are given by

$$\mathrm{Ze}_m=[\mathrm{Je}_m(\xi)+A\mathrm{Ne}_m(\xi)]\mathrm{ce}_m(\eta)\cos(\omega_m t), \tag{16a}$$

$$\mathrm{Zo}_m=[\mathrm{Jo}_m(\xi)+B\mathrm{No}_m(\xi)]\mathrm{se}_m(\eta)\cos(\omega_m t), \tag{16b}$$

where A and B are constants to be determined, $m\geqslant 0$ for even modes, and $m\geqslant 1$ for the odd modes.

The wave solutions (16) must satisfy the Neumann condition at both elliptic boundaries. This condition states that the normal derivatives of Ze_m and Zo_m vanish at each point of the boundaries. For even modes we have $\mathrm{Ze}'_m(\xi_0,\eta,t)=\mathrm{Ze}'_m(\xi_1,\eta,t)=0$, where the prime denotes the derivative with respect to the radial variable ξ. By evaluating the derivative of Eq. (16a) at both elliptic boundaries, we see that the Neumann condition is fulfilled only if

$$\mathrm{Je}'_m(\xi_0;q)+A\mathrm{Ne}'_m(\xi_0;q)=0, \tag{17a}$$

$$\mathrm{Je}'_m(\xi_1;q)+A\mathrm{Ne}'_m(\xi_1;q)=0. \tag{17b}$$

This is a set of two linear equations with a unknown coefficient A. According to linear algebra, a nontrivial solution to this set exists only if the following characteristic equation for the unknown parameter q is satisfied:

$$\mathrm{Je}'_m(\xi_0)\mathrm{Ne}'_m(\xi_1)-\mathrm{Je}'_m(\xi_1)\mathrm{Ne}'_m(\xi_0)=0. \tag{18}$$

This characteristic equation can only be solved numerically.[31] Let us denote $q_{m,n}$ as the nth zero of Eq. (18). Once the value of $q_{m,n}$ has been determined, the corresponding value of A can be calculated using any of the boundary condition equations (17), and thus $A=-\mathrm{Je}'_m(\xi_0;q)/\mathrm{Ne}'_m(\xi_0;q)$. Finally, recalling that $\omega=kv$, the frequency of the mode (m,n) is given by $\omega_{m,n}=[4v^2q_{m,n}/f^2]^{1/2}=[4g\,dq_{m,n}/f^2]^{1/2}$.

For numerical computations, let us choose the values $\xi_1=0.5$ and $\xi_2=1.5$. The eigenvalues of frequency corresponding to the first oscillating modes are listed in Table III in units of $\sqrt{4gd/f^2}$. We can see that the odd modes have lower frequencies than the even modes (${}_o\omega_{m,n}<{}_e\omega_{m,n}$). Note that this behavior is contrary to the results obtained for the modes in the membrane (see Table II), where ${}_e\omega_{m,n}<{}_o\omega_{m,n}$. There is a simple physical explanation for this fact: for the membrane the even modes oscillate without obstruction along the largest axis of the ellipse, whereas the odd modes oscillate along the shorter axis. In the confocal annular elliptic lake the even modes tend to vibrate along the largest axis as well; however, now the internal wall is an obstacle that changes the relative distances. With regard to Fig. 1, let us denote as a' the horizontal separation between the outer and the inner elliptic boundaries along the x axis, and b' the vertical separation along the y axis. We now apply Eq. (2) to show that b' is always greater than a'. We have $a'=a_0-a_1=f\cosh\xi_0\cos(0)-f\cosh\xi_1\cos(0)=f(\cosh\xi_0-\cosh\xi_1)$. Analogously for b' we obtain $b'=f(\sinh\xi_0-\sinh\xi_1)$. The difference $b'-a'$ gives

$$b'-a'=f[(\sinh\xi_0-\cosh\xi_0)-(\sinh\xi_1-\cosh\xi_1)]. \tag{19}$$

By expressing the hyperbolic functions in terms of exponential functions, we can write Eq. (23) in the simpler form

$$b'-a'=\frac{f}{2}[\exp(-\xi_1)-\exp(-\xi_0)]>0. \tag{20}$$

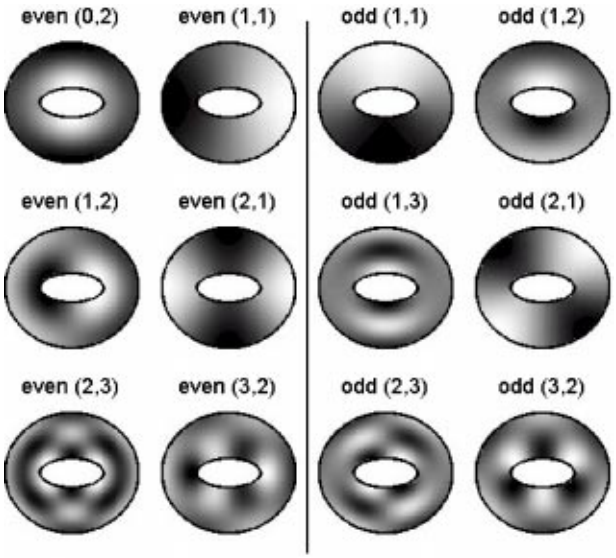

Fig. 7. Plots of the first even and odd standing waves in an confocal annular elliptic lake.

We now can appreciate that b' is greater than a' for any $\xi_0 > \xi_1 > 0$. Hence, the inclusion of an internal elliptic wall leads to even modes to vibrate in shorter distances than odd modes, and consequently ${}_o\omega_{m,n} < {}_e\omega_{m,n}$.

In Fig. 7 we plot several patterns corresponding to the first standing modes. In particular, the mode ${}_{e,o}u_{m,n}$ has $2m(n-1)$ nodal points. In Fig. 8 we show a three-dimensional plot of $\mathrm{Ze}_{12}(\xi,\eta)$. Observe that the Neumann condition is satisfied at both elliptic boundaries.

A. Traveling elliptic waves in the confocal annular elliptic lake

Similar to the propagating waves in a rope, the standing patterns shown in Fig. 7 may be regarded as the result of traveling waves propagating in opposite directions. To be precise, outgoing and incoming elliptic waves propagate radially while reflecting at the elliptic walls.

To understand this traveling behavior of the Mathieu solutions, it should be mentioned that analogous to the Hankel functions $H_m^{(1),(2)}$ occurring in Bessel equations, the solutions of Eq. (4) can be expressed in terms of the even and the odd Mathieu–Hankel functions of the first and second kind

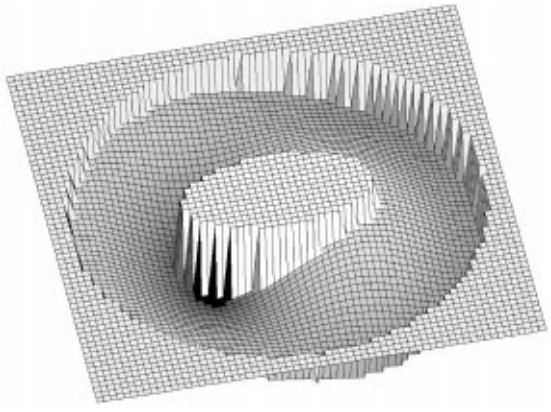

Fig. 8. Surface plot of Ze_{12}. A top view is shown in Fig. 7.

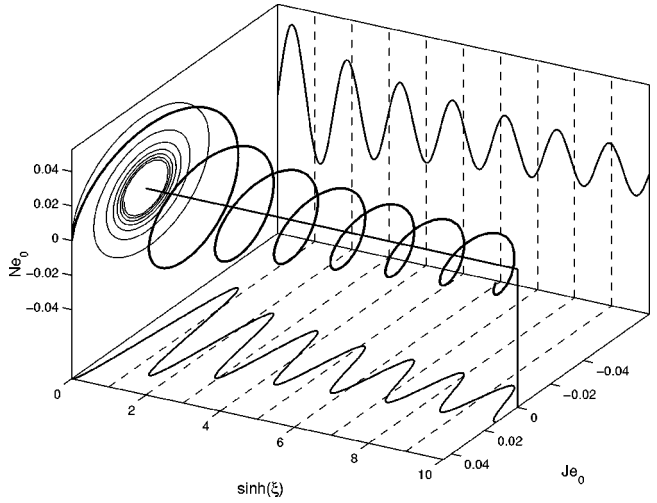

Fig. 9. Evolution of the zero-order Mathieu–Hankel function $\mathrm{Je}_0 + i\mathrm{Ne}_0$ in the complex space. The separation of the three-dimensional curve with respect to the axial axis is the modulus of the function.

$$\mathrm{He}_m^{(1),(2)}(\xi;q) = \mathrm{Je}_m(\xi;q) \pm i\mathrm{Ne}_m(\xi;q), \tag{21a}$$

$$\mathrm{Ho}_m^{(1),(2)}(\xi;q) = \mathrm{Jo}_m(\xi;q) \pm i\mathrm{No}_m(\xi;q), \tag{21b}$$

where the super-index (1) is associated with the positive sign and (2) with the negative one. Similar to the Hankel functions which are often used to represent outgoing and incoming cylindrical waves,[18] the Mathieu–Hankel functions can represent elliptical waves propagating radially in the positive and negative direction of ξ. By making use of these functions, the wave solutions in Eq. (16) can be rewritten in a traveling wave format

$$\mathrm{Ze}_m = \mathrm{He}_m^{(1),(2)}(\xi)\,\mathrm{ce}_m(\eta)\exp(-i\omega_m t), \tag{22a}$$

$$\mathrm{Zo}_m = \mathrm{Ho}_m^{(1),(2)}(\xi)\,\mathrm{se}_m(\eta)\exp(-i\omega_m t), \tag{22b}$$

where the time dependence has been expressed in complex form.

We can more easily visualize the traveling wave behavior by analyzing the asymptotic expansions of the Mathieu–Hankel functions as q increases. For instance, for even functions $\mathrm{He}^{(1),(2)}(\xi,q) \sim v^{-1/2}\exp(\pm iv)$, where $v = \exp(\xi)$. The substitution of this approximation into Eq. (22a) yields

$$\mathrm{Ze}_m \sim \frac{\mathrm{ce}_m(\eta)}{\sqrt{v}}\cos(\pm v - \omega t). \tag{23}$$

Equation (23) can now be recognized as a wave traveling in the positive or negative direction of the coordinate v. We may imagine that the outer boundary reflects the outgoing wave generating an incoming wave. Similarly, the incoming wave is reflected by the inner boundary producing again an outgoing wave. In Fig. 9 we plot the Mathieu–Hankel function $\mathrm{He}_0^{(1)} = \mathrm{Je}_0 + i\mathrm{Ne}_0$ in a three-dimensional complex space. This graphical representation of $\mathrm{He}_0^{(1)}$ is unusual in the literature. Whereas we had to link up in our mind the separate and disconnected characteristics of the real and imaginary parts of the complex function, we can now see the relation at a glance. Observe in the plot the tendency of the RMF to be periodic as the coordinate $\sinh\xi$ increases.

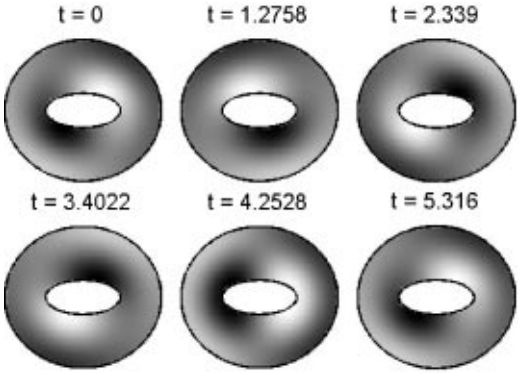

Fig. 10. Plot of the superposition $Z_{12}=\mathrm{Ze}_{12}+\mathrm{Zo}_{12}$ at six different times. The resulting is a anticlockwise rotating wave. The time values are given in $\sqrt{f^2/4\,dg}$ units.

B. Superposition of modes: Rotating waves

We now are interested in the superposition of an even and an odd mode, that is, $Z_{m,n}=\mathrm{Ze}_{m,n}+\mathrm{Zo}_{m,n}$. Because their oscillating frequencies are different, the pattern produced by the superposition varies in time. In Fig. 10 we plot Z_{12} at six increasing times; each constituent mode is plotted separately in Fig. 7. The resulting wave is a rotating perturbation that has angular momentum different from zero.[37]

The cross points between the nodal lines of $\mathrm{Ze}_{m,n}$ and $\mathrm{Zo}_{m,n}$ correspond to nodal points of the resulting wave. If we stay on the water surface at a fixed point on a nodal line, we can observe that this point moves harmonically. Similarly, the motion of any point outside of a nodal line is the superposition of two harmonic motions with different frequencies and amplitudes.

V. CONCLUSIONS

We have graphically presented some properties of the Mathieu functions. Our main goal is to motivate their use and familiarity. As with many other special functions, it is not necessary to know them in great mathematical detail in order to use them in applications. The approach presented here can be used whether one wishes to become familiar with the functions or as a starting point for a deeper analysis. We have illustrated in a diversity of plot types those Mathieu functions that appear more frequently in physical applications.

In our experience, the best way to visualize the behavior of Mathieu functions when one is beginning their study is to think in terms of their more familiar analogies: (a) AMF are analogous to trigonometric functions and (b) the RMF behave like Bessel functions. The variety and peculiarities of these functions are so rich that it is not possible to show them all within this article. Instead, we provide detailed mathematical information and more plots of Mathieu functions via Ref. 38. We believe that the Mathieu functions deserve the attention of the authors of future textbooks on mathematics for scientists and engineers.

ACKNOWLEDGMENTS

The authors are grateful to the reviewers who suggested many improvements to the article. Financial support was provided by the Consejo Nacional de Ciencia y Tecnologia (CONACyT), México.

APPENDIX A: COMPARATIVE NOTATIONS OF MATHIEU FUNCTIONS

As a quick reference for those beginning their study of Mathieu functions, we summarize in Table IV the most common notations used in the literature. The two most common nomenclature conventions for Mathieu functions are those of McLachlan[3] and Morse.[25] McLachlan's nomenclature has its origins in the notation used by the first researchers of the Mathieu functions and is arbitrary. This arbitrariness in the notation, in addition to the existence of different normalizations, often leads to a confusion. Despite this fact, McLachlan's terminology is the most commonly employed notation in the scientific literature. Morse's nomenclature was created by thinking about the connection of each Mathieu function with its corresponding Bessel analogy. From this point of view, Morse's notation is advantageous, because it facilitates the visualization and classification of the Mathieu functions.

Table IV. Comparative notations of the Mathieu functions.

This paper	McLachlan (Ref. 3) Gradshteyn (Ref. 28)	Erdelyi (Ref. 26)	Morse (Ref. 25)	Abramowitz (Ref. 27)	Stratton (Ref. 24)	Refs. 19–23
ce	ce	ce	Se	ce	Se	ce
se	se	se	So	se	So	se
Je	ce	ce	Je	$\mathrm{Mc}^{(1)}$	$\mathrm{Re}^{(1)}$	
Jo	Se	Se	Jo	$\mathrm{Mc}^{(1)}$	$\mathrm{Ro}^{(1)}$	
Ne	Fey	Fey	Ne	$\mathrm{Mc}^{(2)}$	$\mathrm{Re}^{(2)}$	
No	Gey	Gey	No	$\mathrm{Ms}^{(2)}$	$\mathrm{Ro}^{(2)}$	
Ie	$\mathrm{Ce}(-q)$					
Io	$\mathrm{Se}(-q)$					
Ke	Fek					
Ko	Gek					
$\mathrm{He}^{(1),(2)}$	$\mathrm{Me}^{(1),(2)}$	$\mathrm{Me}^{(1),(2)}$	$\mathrm{He}^{(1),(2)}$	$\mathrm{Mc}^{(3),(4)}$	$\mathrm{Re}^{(3),(4)}$	
$\mathrm{Ho}^{(1),(2)}$	$\mathrm{Ne}^{(1),(2)}$	$\mathrm{Ne}^{(1),(2)}$	$\mathrm{Ho}^{(1),(2)}$	$\mathrm{Ms}^{(3),(4)}$	$\mathrm{Ro}^{(3),(4)}$	

APPENDIX B: MATHIEU FUNCTIONS AND THEIR COEFFICIENTS

Because the angular Mathieu functions ce_m and se_m are periodic, they can be expanded in terms of Fourier series. The corresponding expansions fall into four classes, according to their symmetry or antisymmetry, about $\eta=0$ and $\eta=\pi/2$, namely,

$$\mathrm{ce}_{2r}(\eta;q)=\sum_{k=0}^{\infty} A_{2k}(q)\cos[2k\eta], \tag{B1a}$$

$$\mathrm{ce}_{2r+1}(\eta;q)=\sum_{k=0}^{\infty} A_{2k+1}(q)\cos[(2k+1)\eta], \tag{B1b}$$

$$\mathrm{se}_{2r+2}(\eta;q)=\sum_{k=0}^{\infty} B_{2k+2}(q)\sin[(2k+2)\eta], \tag{B1c}$$

$$\mathrm{se}_{2r+1}(\eta;q)=\sum_{k=0}^{\infty} B_{2k+1}(q)\sin[(2k+1)\eta], \tag{B1d}$$

where $r=0,1,2,\ldots$. The recurrence relations between the coefficients can be derived by substituting these series in the Mathieu equation (3). For instance for the functions ce_{2r}, we obtain

$$aA_0=qA_2, \tag{B2a}$$

$$(a-4)A_2=q(2A_0+A_4), \tag{B2b}$$

$$[a-(2k)^2]A_{2k}=q(A_{2k-2}+A_{2k+2}), \tag{B2c}$$

where $k\geqslant 2$.

There are two common approaches to finding the coefficients of the Fourier series. The first one is based on transforming the recurrence relations in Eq. (B2) into continued fractions and to apply further algebraic methods to find the roots; see the details in Refs. 3 and 27. The second method is based on constructing an infinite matrix starting from the recurrence relations. The eigenvalues and eigenvectors of this matrix are the eigenvalues a of the Mathieu equation and the coefficients A of the Fourier series; see the details in Refs. 8 and 9.

The RME in Eq. (4) is obtained from the AME in Eq. (3) by setting the change of variable $\eta=i\xi$. Therefore, we can apply this change of variable to the AMF in [Eq. (B1)] to obtain the following expansions:

$$\mathrm{Je}_{2n}(\xi;q)=\sum_{k=0}^{\infty} A_{2k}(q)\cosh[2k\xi], \tag{B3a}$$

$$\mathrm{Je}_{2n+1}(\xi;q)=\sum_{k=0}^{\infty} A_{2k+1}(q)\cosh[(2k+1)\xi], \tag{B3b}$$

$$\mathrm{Jo}_{2n+2}(\xi;q)=\sum_{k=0}^{\infty} B_{2k+2}(q)\sinh[(2k+2)\xi], \tag{B3c}$$

$$\mathrm{Jo}_{2n+1}(\xi;q)=\sum_{k=0}^{\infty} B_{2k+1}(q)\sinh[(2k+1)\xi]. \tag{B3d}$$

[a]Electronic mail: juliocesar@itesm.mx

[1]L. Ruby, "Applications of the Mathieu equation," Am. J. Phys. **64**, 39–44 (1996).
[2]E. Mathieu, "Le mouvement vibratoire d'une membrane de forme elliptique," J. Math. Pures Appl. **13**, 137–203 (1868).
[3]N. W. McLachlan, *Theory and Application of Mathieu Functions* (Oxford Press, London, 1951).
[4]J. C. Gutiérrez-Vega, M. D. Iturbe-Castillo, and S. Chávez-Cerda, "Alternative formulation for invariant optical fields: Mathieu beams," Opt. Lett. **25**, 1493–1495 (2000).
[5]J. C. Gutiérrez-Vega, M. D. Iturbe-Castillo, G. A. Ramírez, E. Tepichín, R. M. Rodríguez-Dagnino, S. Chávez-Cerda, and G. H. C. New, "Experimental demonstration of optical Mathieu beams," Opt. Commun. **195**, 35–40 (2001).
[6]P. N. Shivakumar and J. Xue, "On the double points of a Mathieu equation," J. Comput. Appl. Math. **107**, 111–125 (1999).
[7]A. Lindner and H. Freese, "A new method to compute Mathieu functions," J. Phys. A **27**, 5565–5571 (1994).
[8]F. A. Alhargan, "Algorithm for the computation of all Mathieu functions of interger orders," ACM Trans. Math. Softw. **26**, 390–407 (2001).
[9]D. Frenkel and R. Portugal, "Algebraic methods to compute Mathieu functions," J. Phys. A **34**, 3541–3551 (2001).
[10]J. C. Gutiérrez-Vega, S. Chávez-Cerda, and R. M. Rodríguez-Dagnino, "Free oscillations in an elliptic membrane," Rev. Mex. Fis. **45**, 613–622 (1999).
[11]S. Li and B. S. Wang, "Field expressions and patterns in elliptical waveguides," IEEE Trans. Microwave Theory Tech. **48**, 864–867 (2000).
[12]T. R. Carver, "Mathieu's functions and electrons in a periodic lattice," Am. J. Phys. **39**, 1225–1231 (1971).
[13]R. C. Cross, "Demonstration of wave propagation in a periodic structure," Am. J. Phys. **53**, 563–567 (1985).
[14]T. Pradhan and A. V. Khare, "Plane pendulum in quantum mechanics," Am. J. Phys. **41**, 59–66 (1973).
[15]R. Aldrovandi and P. Leal Ferreira, "Quantum pendulum," Am. J. Phys. **48**, 660–664 (1980).
[16]G. L. Baker, J. A. Blackburn, and H. J. T. Smith, "The quantum pendulum: Small and large," Am. J. Phys. **70**, 525–531 (2002).
[17]M. B. Robertson and U. Köhler, "Physiological flow waveform in a rigid elliptical vessel," IMA J. Math. Appl. Med. Biol. **18**, 77–98 (2001).
[18]G. Arfken and H. Weber, *Mathematical Methods for Physicists*, 5th ed. (Academic, San Diego, 2001).
[19]D. Richards, *Advanced Mathematical Methods* (Cambridge University Press, Cambridge, 2002).
[20]J. Mathews and R. L. Walker, *Mathematical Methods of Physics*, 2nd ed. (Benjamin, New York, 1970), Chap. 7.
[21]H. Jeffreys and B. Jeffreys, *Methods of Mathematical Physics*, 3rd ed. (Cambridge University Press, Westford, MA, 1972), Chap. 16.
[22]E. T. Whittaker and G. N. Watson, *A Course of Modern Analysis*, 4th ed. (Cambridge University Press, Westford, MA, 1927), Chap. 19.
[23]E. L. Ince, *Ordinary Differential Equations* (Dover, New York, 1967), Chap. 20.
[24]J. A. Stratton, *Electromagnetic Theory* (McGraw-Hill, New York, 1941), Chap. 6.
[25]P. M. Morse and H. Feshbach, *Methods of Theoretical Physics* (McGraw-Hill, New York, 1953), Chap. 6.
[26]A. Erdélyi, *Bateman Manuscript Project on Higher Transcendental Functions* (McGraw-Hill, Malabar, FL, 1981), Chap. 16.
[27]M. Abramowitz and I. Stegun, *Handbook of Mathematical Functions* (Dover, New York, 1964), Chap. 20.
[28]I. S. Gradshteyn and I. M. Ryzhik, *Table of Integral Series and Products*, 6th ed. (Academic, London, 2000), Chap. 8.
[29]E. Jahnke and F. Emde, *Tables of Functions* (Dover, New York, 1945), Chap. 11.
[30]Because of the periodic behavior of the AMF, these functions are often referred to as *periodic Mathieu functions* (Ref. 19).
[31]Numerical libraries for computing the Mathieu functions (in particular the radial ones) are not readily available; for this reason, we have developed our own numerical routines based on the theory of Mathieu functions. Roughly speaking, we applied matrix methods (Refs. 7, 8, and 19) to find the eigenvalues a_m of the Mathieu equations. Afterward, the AMF are computed applying Fourier series, whereas Bessel-function-product-series were used to evaluate the RMF (Refs. 3, 19, and 27). A very practical list of properties and formulas of expansion series of Mathieu functions is supplied by Gradshteyn (Ref. 28). We compared our results with those from recent papers (Refs. 8, 9), and an accuracy of more than 10^{-9} was obtained. The roots of the characteristic equations (18) were calculated

using a Newton–Raphson method. We have taken advantage of the graphical facilities of Matlab to show the plots of Mathieu functions.
[32]H. Waalkens, J. Wiersig, and H. R. Dullin, ''Elliptic quantum billiard,'' Ann. Phys. (N.Y.) **260**, 50–90 (1997).
[33]Second radial functions Ne_m and No_m are excluded because the wave solutions and their derivatives must to be continuous at $\xi=0$. See Fig. 4.
[34]The modes in circular membranes are well studied in textbooks (Ref. 18). The natural frequencies are given by $\omega_{m,n}=(F/\sigma)^{1/2}r_{m,n}/a$, where $r_{m,n}$ is the nth root of the J_m Bessel function, a is the radius, and F and σ were defined in Sec. III.
[35]H. Jeffreys, ''The free oscillations of water in an elliptical lake,'' Proc. London Math. Soc. **23**, 455–476 (1924).
[36]S. Goldstein, ''The free oscillations of water in a canal of elliptic plan,'' Proc. London Math. Soc. **28**, 91–101 (1927).
[37]P. H. Cerpeley, ''Rotating waves,'' Am. J. Phys. **60**, 938–942 (1992).
[38]http://homepages.mty.itesm.mx/jgutierr/mathieu.htm

Bladder Glass. Nineteenth century students saw many demonstrations involving the effects of atmospheric pressure. In the bladder glass, a piece of animal bladder is tied with twine over the top of a vessel open at both ends. The lower end is placed on the bottom plate of a vacuum pump, and only a few strokes of the pump are needed to produce a pressure differential of essentially one atmosphere. The bladder bursts inward with a bang loud enough to wake the sleepers in the back of the classroom. This demonstration was last done at Washington and Lee University about 1900, and then it was set aside until I discovered it eighty years later. (Photograph and notes by Thomas B. Greenslade, Jr., Kenyon College)